

Dynamics of the Dorsal morphogen gradient

Jitendra S. Kanodia^a, Richa Rikhy^b, Yoosik Kim^a, Viktor K. Lund^c, Robert DeLotto^c, Jennifer Lippincott-Schwartz^{b,1}, and Stanislav Y. Shvartsman^{a,1}

^aDepartment of Chemical Engineering and Lewis-Sigler Institute for Integrative Genomics, Princeton University, Washington Road, Princeton, NJ 08544;

^bCell Biology and Metabolism Branch, NIH, Building 32, 18 Library Drive, Bethesda, MD 20892; and ^cDepartment of Molecular Biology, University of Copenhagen, Ole Maaløes Vej 5, DK-2200 Copenhagen, Denmark

Contributed by Jennifer Lippincott-Schwartz, October 28, 2009 (sent for review September 6, 2009)

The dorsoventral (DV) patterning of the *Drosophila* embryo depends on the nuclear localization gradient of Dorsal (Dl), a protein related to the mammalian NF- κ B transcription factors. Current understanding of how the Dl gradient works has been derived from studies of its transcriptional interpretation, but the gradient itself has not been quantified. In particular, it is not known whether the Dl gradient is stable or dynamic during the DV patterning of the embryo. To address this question, we developed a mathematical model of the Dl gradient and constrained its parameters by experimental data. Based on our computational analysis, we predict that the Dl gradient is dynamic and, to a first approximation, can be described as a concentration profile with increasing amplitude and constant shape. These time-dependent properties of the Dl gradient are different from those of the Bicoid and MAPK phosphorylation gradients, which pattern the anterior and terminal regions of the embryo. Specifically, the gradient of the nuclear levels of Bicoid is stable, whereas the pattern of MAPK phosphorylation changes in both shape and amplitude. We attribute these striking differences in the dynamics of maternal morphogen gradients to the differences in the initial conditions and chemistries of the anterior, DV, and terminal systems.

computational modeling | *Drosophila* | systems biology | parameter estimation

A tissue patterned by morphogen gradients can change its transcriptional state, grow, or deform either in response to the gradients or independently of them (1–3). When these changes are much slower than the dynamics of the gradient, a tissue responds to a stable signal. Transcriptional interpretation of such signals can rely on differences in the expression thresholds of target genes with respect to the spatially distributed repressors or activators (2, 4). A different strategy for signal interpretation is required when the formation of positional information becomes intertwined with the dynamics of the patterned system (2, 5). Here, we suggest that the dorsoventral (DV) patterning of the *Drosophila* embryo operates in this regime.

The DV patterning of the *Drosophila* embryo depends on the nuclear localization gradient of Dorsal (Dl), a protein related to the NF- κ B family of transcription factors (6–10). Transcriptional interpretation of the Dl gradient depends on the differences in the affinities of the Dl binding sites in the Dl-target genes and several gene expression and signaling cascades initiated by Dl (6, 11, 12). A ventral-to-dorsal occupancy gradient of the Toll cell surface receptor provides the activating signal for the DV patterning (13). In the absence of this signal, Dl is sequestered in the cytoplasm, in complex with an inhibitory protein I- κ B, called Cactus (Cact) in *Drosophila*. In response to Toll signaling, the Dl–Cact complex dissociates, Cact is degraded, and Dl enters the nucleus to control gene expression. In the current model of DV patterning, positional information is established by the spatial pattern of Toll occupancy (13, 14).

The Dl gradient forms during the last five nuclear divisions in a syncytial blastoderm, a single cell with multiple nuclei (15). Because nuclei can be viewed as competing with Cact for Dl, an increase in the number of nuclei can influence the Dl gradient, but whether or not this happens is currently unknown. Dl undergoes rapid nucleocytoplasmic shuttling with a nuclear residence time of

several minutes (16). Nuclei change in volume and undergo five synchronous divisions (15, 17). To explore how these processes contribute to the formation of the Dl gradient, we formulated a mathematical model that accounts for the nuclear import and export of Dl, its interaction with Cact, and the dynamics of nuclear density and volumes in the syncytial blastoderm. Based on the computational analysis of this model and a number of our model-based experiments, we argue that the Dl gradient is dynamic and, to a first approximation, can be described as a spatial pattern with constant shape and increasing amplitude.

Results

At the outset of this work, the only quantitative information about the spatial distribution of nuclear Dl could be found in the study by Zinzen et al. (18), who had characterized the DV pattern of nuclear Dl at a single time point. The domains of the Dl-target genes begin to form several nuclear cycles before cellularization, and it is important to determine whether these genes respond to a constant or time-dependent signal. This question has been prompted by recent studies of the anterior-posterior (AP), DV, and terminal systems. First, the nuclear levels of Bcd, a morphogen that specifies the anterior structures of the embryo, are stable throughout the last five syncytial nuclear divisions. Bcd undergoes nucleocytoplasmic shuttling on the time scale of several minutes. After mitosis, the nuclear levels of Bcd drop to zero, but are then rapidly reestablished to the premitosis level. Thus, with the exception of a rapid transient associated with nuclear divisions, a particular point in the embryo is exposed to a constant level of nuclear Bcd, which is distributed in a spatial pattern with constant shape and amplitude. In contrast, the pattern of phosphorylated ERK/MAPK (dpERK), which specifies the terminal regions of the embryo, changes in both shape and amplitude. Over the five last nuclear divisions in the syncytial blastoderm, the nuclear levels of dpERK increase at the poles and decrease in the midbody of the embryo.

We asked whether the spatial pattern of nuclear localization of Dl is stable, similar to the pattern of Bcd, or dynamic, similar to the pattern of dpERK. Answering this question requires quantitative characterization of the nuclear levels of Dl along the DV axis and at multiple time points. Here, this goal is achieved using a combination of quantitative imaging and mathematical modeling of the biophysical processes associated with the DV patterning of the embryo. Our experimental and computational results reveal that the DV pattern of nuclear Dl behaves differently from both the Bcd and dpERK gradients. Similar to Bcd, the shape of the DV pattern of nuclear Dl has approximately constant shape, but the amplitude of this pattern increases with time.

To visualize the DV distribution of nuclear Dl, we used a transgenic line where one endogenous copy of *dl* was replaced by

Author contributions: J.S.K., R.R., Y.K., R.D., J.L.-S., and S.Y.S. designed research; J.S.K., R.R., Y.K., and S.Y.S. performed research; J.S.K., R.R., Y.K., V.K.L., J.L.-S., and S.Y.S. analyzed data; and J.S.K., J.L.-S., and S.Y.S. wrote the paper.

The authors declare no conflict of interest.

¹To whom correspondence may be addressed. E-mail: jlippin@helix.nih.gov or stas@princeton.edu.

This article contains supporting information online at www.pnas.org/cgi/content/full/0912395106/DCSupplemental.

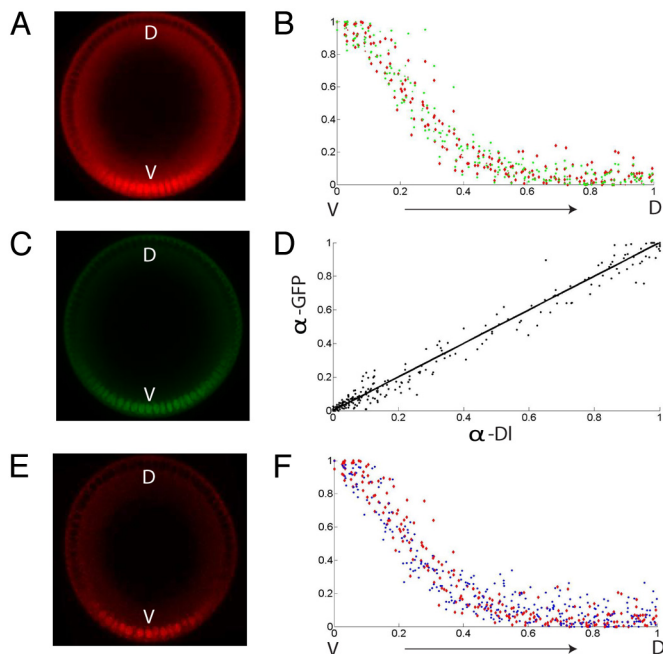


Fig. 1. Validation of the *dl-GFP* transgenic line using imaging of fixed embryos. (*A* and *B*) End-on imaging of transgenic embryos costained with α -DI (*A*) and α -GFP (*B*) antibodies. In *A*, *C*, and *E* the cross-sections of the embryos are oriented with the dorsal side up, and cycle-14 embryos are shown (XY scale is 150 microns). (*C*) Comparing the normalized gradients of α -DI (red) and α -GFP (green) intensity levels in six embryos. (*D*) Plot of α -DI intensity vs. α -GFP intensity in six embryos. (*E*) End-on imaging of the wild-type embryos stained with α -DI antibodies. (*F*) Comparing the normalized gradients of α -DI intensity levels in eight wild-type embryos (blue) and six transgenic embryos (red).

a *dl-gfp* transgene (see *Materials and Methods*). Several control experiments were done to test whether the DI gradient, quantified from the GFP signal in this line is close to the DI gradient obtained by quantifying the wild-type α -DI antibody stainings. First, fixed embryos were stained with α -DI and α -GFP antibodies and the fluorescent intensities of the nuclear α -DI and α -GFP stainings were compared with each other (Fig. 1*A–D*). As shown in Fig. 1*D*, there is a strong linear correlation between the intensities of the α -DI and α -GFP antibody stainings. Thus, except for the differences in the background levels, the DV pattern of nuclear DI obtained on the basis of the GFP staining is proportional to the pattern that is based on the α -DI antibody staining. Because the α -DI antibody detects both endogenous and GFP-tagged DI, whereas the α -GFP antibody detects only GFP-tagged DI, the linear correlation suggests that the GFP tag does not significantly interfere with the normal processes of DI transport and interactions. As an additional control experiment, we used the α -DI antibody and stained the wild-type embryos together with embryos with one wild-type and one GFP-tagged copy of *dl* (Fig. 1*E*). Comparison of the nuclear DI gradients in the wild-type and transgenic embryos (Fig. 1*F*) indicates that they are very close to each other. Thus, the line with one wild-type and one GFP-tagged *dl* can be used to monitor the dynamics of the DI gradient in live imaging experiments.

To follow the dynamics of the DV pattern of nuclear DI, we used the “end on” imaging technique (19), where embryos are mounted with their AP axis perpendicular to the horizontal surface, enabling the imaging along the DV axis of the embryo. The space–time plot of nuclear DI extracted from a live-imaging experiment with >130 time points between cycles 11 and 14 is shown in Fig. 2*A*. The gradient of nuclear DI is very dynamic. Concentration of nuclear DI increases during interphase, which is followed by a drop to a low

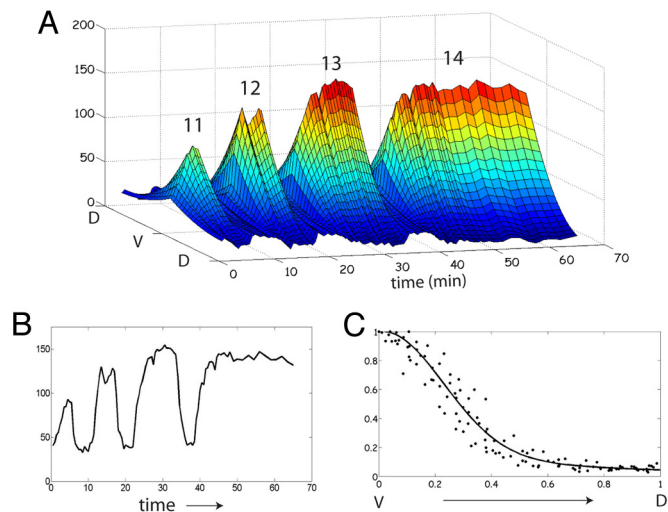


Fig. 2. Live imaging of the DI gradient. (*A*) An interpolated surface plot of the nuclear DI-GFP levels along the DV axis at ≈ 130 time points during nuclear division cycles 11–14. (*B*) Dynamics of the nuclear DI level at the ventral-most point of the embryo. (*C*) The average gradient (line) at 15 min in cycle 14 obtained from four live-imaging experiments (dots).

value during mitosis and a subsequent increase during the next cycle (Fig. 2*A* and *B*).

One of the main sources of variability in the end-on imaging of the DI gradient is introduced by the movement of nuclei in and out of the focal plane, both during interphase and between different nuclear division cycles. The inherent dynamics of the arrangement of the nuclei induces large variability in the profiles of the DI gradients along the DV axis. This effect, which is particularly significant during the earlier nuclear division cycles, makes the quantitative analysis of the DI gradients during these cycles extremely challenging. At the same time, the arrangement of nuclei is much more regular during cycle 14, when they are tightly packed under the plasma membrane. Thus, we use cycle-14 data from four separate live imaging experiments to extract the DV pattern of nuclear DI at a fixed time point: ≈ 15 min into cycle 14 (Fig. 2*C*). To characterize the dynamics of the DV pattern of nuclear DI at the previous time points, we use the data in Fig. 2*C* as a quantitative constraint for the mathematical model that accounts for the dynamics of DI/Cact interactions and nuclear divisions.

The objective of our model is to characterize the dynamics of the DV pattern of nuclear DI during the last five syncytial cell cycles. We model the syncytium as a periodic arrangement of cuboidal compartments, each of which contains a single spherical nucleus and an associated cytoplasmic region (Fig. 3*A*). DI, Cact, and DI–Cact complex diffuse rapidly within each of the compartments and undergo slow exchange with the neighboring compartments. The kinetic part of our model is a subset of reactions included in the more detailed models of the mammalian NF- κ B system (Fig. 3*B*) (20). The association of DI and Cact is modeled as a second-order reaction with a spatially uniform rate constant. The dissociation of the DI–Cact complex is modeled as a first-order process with a rate constant that depends on the DV position, reflecting a DV pattern of Toll activation. We assume that this pattern remains constant during the entire patterning process. The rates of the nuclear import and export of DI depend on the surface area of the nucleus. Finally, we assume free Cact is produced at a constant rate and degraded in a first-order reaction.

Within each nuclear cycle nuclear radius increases (17). As a consequence of this change, nuclear and cytoplasmic concentrations are affected by both the chemical processes and volume changes. At specific time intervals that correspond to the detailed measurements of Foe and Alberts (15), nuclei divide. During

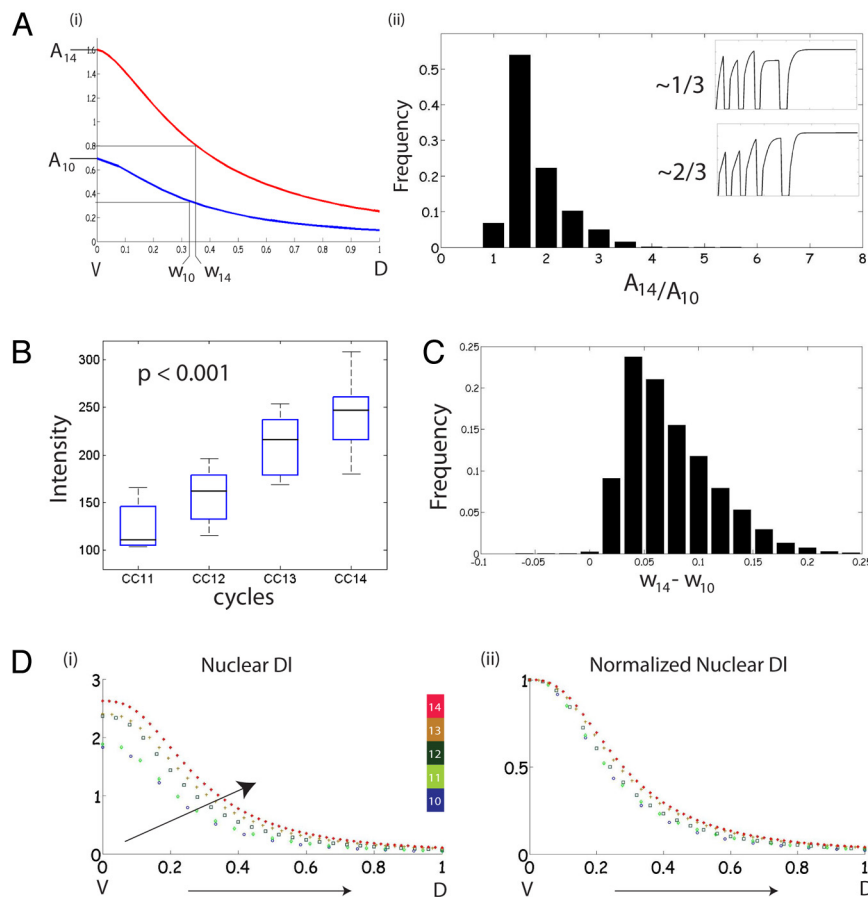


Fig. 5. Statistical analysis of model predictions. (A) (i) Schematic of nuclear DI gradients at cycles 10 and 14; the lines correspond to the amplitude of the gradient (A_{10} and A_{14}) and the width of the gradient at half-peak amplitude (w_{10} and w_{14}). (ii) Distribution of the ratio of the amplitudes of nuclear DI gradient at cycles 14 and 10, computed on the basis of the ensemble of parameter vectors. Approximately one-third of parameter sets predict multiple combinations of increase and decrease in nuclear DI level at the end of each cycle (*Upper Inset*), while the other two-thirds of the parameter sets predict an ordered increase in nuclear DI level from one cycle to another (*Lower Inset*). (B) Experimental results for the amplitude of nuclear DI gradients at the ventral-most point of the embryo for cycles 11–14. (C) Model-based distribution function of the changes in the half-widths (width of gradient at half-peak amplitude) of the DI gradients, cycles 14 to 10; half-width is defined in A). The distribution shows a peak at 0.05, indicating that the half-width remains almost constant. (D) The DI gradient has constant shape and increasing amplitude. (i) Nuclear DI at different cycles. (ii) Nuclear DI gradient at different cycles with its amplitude normalized to one at the ventral-most end.

which are formed in the same medium and at the same time as the DI gradient (29). Specifically, neither the shape nor the amplitude of the nuclear levels of Bcd are affected by changes in the number of nuclei. The two-peaked pattern of dpERK, however, changes in both shape and amplitude.

What is the origin of these striking differences between the dynamics of the three gradients? The terminal and DV gradients are initiated only when nuclei have reached the plasma membrane and respond to signals from the activated cell surface receptors. At the same time, the functional Bcd gradient is already established at this stage (30). Thus, the stability of the nuclear Bcd gradient during the last five nuclear divisions can be due to the fact that this gradient starts to form earlier and is not affected by nuclei, which sample only a small fraction of total Bcd at any given point along the AP axis (17, 31). Another key factor is the difference in the “chemistries” of Bcd, DI, and dpERK molecules. We have previously proposed that Bcd is not degraded on the time scale relevant for the formation of the gradient (31). In contrast, the molecules that pattern the DV and terminal regions are reactive: DI interacts with Cact and dpERK is dephosphorylated. Both of these processes can be affected by changes in nuclear density. Why, then, does the same change in nuclear density lead to different changes in the DI and dpERK gradients?

We attribute the fact that amplification of the dpERK levels is restricted to the poles, whereas the nuclear DI levels increase everywhere, to the different spatial extents of the sources that activate the DV and terminal systems. Our recent experiments suggest that the occupancy of the Torso receptor, which activates MAPK, is sharply localized to the poles and that the formation of the dpERK gradient relies on the diffusion of activated MAPK to the midbody regions (23, 32). By decreasing the distance to which the dpERK molecule can diffuse before being trapped or dephosphorylated, an increase in the nuclear density can prevent the lateral transport of dpERK to the midbody regions and amplify its level at the poles. However, we argue that a significant fraction of nuclei along the DV axis are exposed to appreciable levels of Toll signaling. As a consequence, lateral movement of the intracellular signaling components is less important for the DV patterning than for patterning of the terminal system, which agrees with the imaging experiments that revealed a slow DI exchange between the adjacent cytoplasmic regions (16).

Understanding how a dynamic DI gradient specifies multiple gene expression boundaries along the DV axis requires quantitative studies of the dynamics of other patterning signals in the early embryo (18, 33–37). As an example, we discuss the expression of genes that are expressed in the ventral and lateral regions of the embryo. Consider the regulation of *sog*, a gene repressed in the

prospective mesoderm and expressed in more lateral regions. It is possible that the ventral boundary of this pattern is stabilized by the feed-forward loop that is induced by Dl and relies on the positive autoregulation of Twist, a high threshold target of Dl (18). If this network operates in a bistable regime, then its output, and hence the ventral boundary of *sog*, can be stable even with increasing levels of Dl. The dorsal boundary, however, depends on the joint regulation of *sog* by both Dl and Zelda, a maternally provided activator of early zygotic transcription (38, 39). We speculate that the dorsal boundary of the *sog* pattern is stabilized by the combined effect of the temporally increasing levels of spatially distributed Dl and decreasing levels of spatially uniform Zelda. Thus, increasing levels of nuclear Dl can be important for the dynamic expression of Dl-target genes. Direct tests of this prediction can rely on the combined experimental, modeling, and computational strategy described in this work.

Materials and Methods

Fly Lines. Dorsal mutants *dl*¹ and *dl*⁴ were obtained from the Bloomington Stock Center at the Indiana University and crossed with the *dl*-GFP/TM3 line. Live imaging was performed with embryos of the genotype *dl*^{1/+}; *p*[*w*+*-dl*-GFP]/+.

Antibody Staining and Live Imaging. Embryos were dechorionated in bleach for 1 min and then washed in 0.7% NaCl containing 0.05% Triton X-100. They were then treated with heptane for 30 s and fixed in a 1:1 mixture of heptane/4% paraformaldehyde in PBS for 20 min at room temperature. After fresh heptane was added, embryos were devitelinized in equal volumes of methanol and stored in methanol at -20°C . For immunostaining, embryos were rehydrated for 10 min in PBS with 0.3% Triton X-100 (PBT) and blocked for 1 h with 2% BSA in PBT at room temperature; this was followed by a 2-h incubation with the primary antibody. The primary antibodies used were mouse anti-Dorsal 7A4 (Developmental Studies Hybridoma Bank at the University of Iowa) at 1:50 and rabbit

anti-GFP (Molecular Probes) at 1:1,500. Embryos were washed in PBT and subsequently stained with fluorescently coupled secondary antibodies (Molecular Probes). For end-on imaging, embryos were mounted on their posterior pole and imaged as described (19).

Embryos were imaged at $\approx 70\ \mu\text{m}$ from the posterior pole, at a position where the diameter of the embryo was $\approx 140\text{--}150\ \mu\text{m}$. Control embryos for secondary background, wild-type embryos, and *dl*1;GFP-dorsal embryos were immunostained on the same day and imaged under the same settings of the confocal microscope. For quantification, small regions of interest were drawn in the nuclei marked by Hoechst dye (Molecular Probes) using the software Image J. Average fluorescence intensity with corresponding positions of nuclei was obtained for anti-Dl and anti-GFP. The gradients were normalized between zero and one by subtracting the minimum intensity measurement within a nucleus and then dividing the entire gradient by the maximum intensity.

Live imaging was performed with *dl*1 heterozygous embryos expressing GFP-dorsal (*dl*^{1/+}; *p*[*w*+*-GFP*-dorsal]/+) to match the wild-type *dl* copy number. Flies were allowed to lay embryos for 1 h at 25 $^{\circ}\text{C}$ on grape juice agar plates. Embryos were dechorionated and mounted on their posterior pole in Lab Tek chambers coated with silane (40), immersed in PBS, and imaged on an LSM 510 confocal microscope. Imaging was performed at $\approx 70\ \mu\text{m}$ from the posterior pole. Quantification was performed with Image J.

For lateral imaging of fixed embryos, they were dechorionated for 1 min in 100% bleach, fixed for 20 min by gentle shaking on a nutator, and devitelinized by vigorous 1-min shaking in a mixture of heptane and methanol. Next, embryos were quickly rehydrated and transferred to the blocking and antibody steps of the protocol. All further processing was done with 0.02% PBS-Triton X-100 as the diluting solution. Dl antibody (Developmental Hybridoma Bank) was used in 1:100 dilution, and goat anti-mouse Alexa Fluor 546 antibody (Invitrogen; 1:500 dilution) was used as a secondary antibody. Imaging was done on a Zeiss LSM510 confocal microscope, with a Zeiss 20 \times (NA 0.6) A-plan objective.

ACKNOWLEDGMENTS. We thank Tsuyoshi Hirashima for help with image processing; Dmitry Papatsenko, Christine Rushlow, Ruth Steward, and Mike Levine for helpful discussions; and Christine Sample, Miriam Osterfield, Alistair Boettiger, and Lily Cheung Chang for critical reading of the manuscript.

- Lander AD (2007) Morpheus unbound: Reimagining the morphogen gradient. *Cell* 128:245–256.
- Ibanes M, Belmonte JCI (2008) Theoretical and experimental approaches to understand morphogen gradients. *Mol Syst Biol* 4:176.
- Jaeger J, Irons D, Monk N (2008) Regulative feedback in pattern formation: Toward a general relativistic theory of positional information. *Development* 135:3175–3183.
- Ashe HL, Briscoe J (2006) The interpretation of morphogen gradients. *Development* 133:385–394.
- Bergmann S, et al. (2007) Presteady-state decoding of the bicoid morphogen gradient. *PLoS Biol* 5:232–242.
- Hong JW, Hendrix DA, Papatsenko D, Levine MS (2008) How the Dorsal gradient works: Insights from postgenome technologies. *Proc Natl Acad Sci USA* 105:20072–20076.
- Roth S, Stein D, Nusslein-Volhard C (1989) A gradient of nuclear localization of the Dorsal protein determines dorsoventral pattern in the *Drosophila* embryo. *Cell* 59:1189–1202.
- Rushlow CA, Han KY, Manley JL, Levine M (1989) The graded distribution of the Dorsal morphogen is initiated by selective nuclear import transport in *Drosophila*. *Cell* 59:1165–1177.
- Steward R (1989) Relocalization of the Dorsal protein from the cytoplasm to the nucleus correlates with its function. *Cell* 59:1179–1188.
- Hoffmann A, Baltimore D (2006) Circuitry of nuclear factor κB signaling. *Immunol Rev* 210:171–186.
- Stathopoulos A, Levine M (2002) Dorsal gradient networks in the *Drosophila* embryo. *Dev Biol* 246:57–67.
- Chopra VS, Levine M (2009) *Combinatorial Patterning Mechanisms in the Drosophila Embryo: Briefings in Functional Genomics and Proteomics* Vol 8, No 4. 243–249.
- Moussian B, Roth S (2005) Dorsoventral axis formation in the *Drosophila* embryo: Shaping and transducing a morphogen gradient. *Curr Biol* 15:R887–899.
- Stathopoulos A, Levine M (2002) Linear signaling in the Toll-Dorsal pathway of *Drosophila*: Activated Pelle kinase specifies all threshold outputs of gene expression while the bHLH protein twist specifies a subset. *Development* 129:3411–3419.
- Foe VE, Alberts BM (1983) Studies of nuclear and cytoplasmic behavior during the 5 mitotic cycles that precede gastrulation in *Drosophila* embryogenesis. *J Cell Sci* 61:31–70.
- DeLotto R, DeLotto Y, Steward R, Lippincott-Schwartz J (2007) Nucleocytoplasmic shuttling mediates the dynamic maintenance of nuclear Dorsal levels during *Drosophila* embryogenesis. *Development* 134:4233–4241.
- Gregor T, Wieschaus E, McGregor AP, Bialek W, Tank DW (2007) Stability and nuclear dynamics of the bicoid morphogen gradient. *Cell* 130:141–153.
- Zinzen RP, Senger K, Levine M, Papatsenko D (2006) Computational models for neurogenic gene expression in the *Drosophila* embryo. *Curr Biol* 16:1358–1365.
- Witzberger M, Fitzpatrick JAJ, Crowley JC, Minden JS (2008) End-on imaging: A new perspective on dorsoventral development in *Drosophila* embryos. *Dev Dyn* 237:3252–3259.
- Cheong R, Hoffmann A, Levchenko A (2008) Understanding NF- κB signaling via mathematical modeling. *Mol Syst Biol* 4:192.
- Gutenkunst RN, et al. (2007) Universally sloppy parameter sensitivities in systems biology models. *PLoS Comput Biol* 3:1871–1878.
- Coley DA (1999) *An Introduction to Genetic Algorithms for Scientists and Engineers* (World Scientific).
- Coppey M, Boettiger AN, Berezhkovskii AM, Shvartsman SY (2008) Nuclear trapping shapes the terminal gradient in the *Drosophila* embryo. *Curr Biol* 18:915–919.
- Markstein M, et al. (2004) A regulatory code for neurogenic gene expression in the *Drosophila* embryo. *Development* 131:2387–2394.
- Papatsenko D, Levine M (2005) Quantitative analysis of binding motifs mediating diverse spatial readouts of the Dorsal gradient in the *Drosophila* embryo. *Proc Natl Acad Sci USA* 102:4966–4971.
- Chen G, Handel K, Roth S (2000) The maternal NF- κB /Dorsal gradient of *Tribolium castaneum*: Dynamics of early dorsoventral patterning in a short-germ beetle. *Development* 127:5145–5156.
- da Fonseca RN, et al. (2008) Self-regulatory circuits in dorsoventral axis formation of the short-germ beetle *Tribolium castaneum*. *Dev Cell* 14:605–615.
- Crocker J, Tamori Y, Erives A (2008) Evolution acts on enhancer organization to fine-tune gradient threshold readouts. *PLoS Biol* 6:2576–2587.
- Shvartsman SY, Coppey M, Berezhkovskii AM (2008) Dynamics of maternal morphogen gradients in *Drosophila*. *Curr Opin Genet Dev* 18:342–347.
- Lucchetta EM, Vincent ME, Ismagilov RF (2008) A precise Bicoid gradient is nonessential during cycles 11–13 for precise patterning in the *Drosophila* blastoderm. *PLoS One* 3:e3651.
- Coppey M, Berezhkovskii AM, Kim Y, Boettiger AN, Shvartsman SY (2007) Modeling the Bicoid gradient: Diffusion and reversible nuclear trapping of a stable protein. *Dev Biol* 312:623–630.
- Berezhkovskii AM, Coppey M, Shvartsman SY (2009) Signaling gradients in cascades of two-state reaction-diffusion systems. *Proc Natl Acad Sci USA* 106:1087–1092.
- Umulis DM, Serpe M, O'Connor MB, Othmer HG (2006) Robust, bistable patterning of the dorsal surface of the *Drosophila* embryo. *Proc Natl Acad Sci USA* 103:11613–11618.
- Mizutani CM, et al. (2005) Formation of the BMP activity gradient in the *Drosophila* embryo. *Dev Cell* 8:915–924.
- Mizutani CM, Meyer N, Roelink H, Bier E (2006) Threshold-dependent BMP-mediated repression: A model for a conserved mechanism that patterns the neuroectoderm. *PLoS Biology* 4:1777–1788.
- Stathopoulos A, Levine M (2005) Localized repressors delineate the neurogenic ectoderm in the early *Drosophila* embryo. *Dev Biol* 280:482–493.
- Von Ohlen T, Doe CQ (2000) Convergence of dorsal, Dpp, and Egr signaling pathways subdivides the *Drosophila* neuroectoderm into three dorsal-ventral columns. *Dev Biol* 224:362–372.
- Liang HL, et al. (2008) The zinc-finger protein Zelda is a key activator of the early zygotic genome in *Drosophila*. *Nature* 456:400–467.
- Liberman LM, Stathopoulos A (2009) Design flexibility in *cis*-regulatory control of gene expression: Synthetic and comparative evidence. *Dev Biol* 327:578–589.
- Mavrakis M, Rikhy R, Lilly M, Lippincott-Schwartz J (2008) Fluorescence imaging techniques for studying *Drosophila* embryo development. *Curr Protoc Cell Biol* 39:4.18.1–43.